Themistos, C., Rahman, B. M., Markides, C., Uthman, M., Quadir, A. & Kejalakshmy, N. (2014). Characterization of graphene-based devices for THz Systems. In: Terahertz Physics, Devices, and Systems VIII: Advanced Applications in Industry and Defense. . SPIE. ISBN 9781628410396

Characterization of graphene-based devices for THz Systems

Christos Themistos*[a], B. M. Azizur Rahman[b], Christos Markides[a],
Md. Uthman[b], A. Quadir[b], N. Kejalakshmy[a]
[a]School of Engineering and Applied Sciences, Frederick University, Nicosia, Cyprus;
[b]School of Engineering and Mathematical Sciences, City University London, UK

ABSTRACT

The H-field finite element method (FEM) based full-vector formulation is used in the present work to study the vectorial modal field properties and the complex propagation characteristics of Surface Plasmon modes of a hollow-core dielectric coated rectangular waveguide structures, and graphene based structures. Additionally, the finite difference time domain (FDTD) method is used to estimate the dispersion parameters and the propagation loss of such waveguides and devices.

Keywords: Finite-element method (FEM), finite-difference time-domain method (FDTD), surface plasmon polariton (SPP), terahertz, graphene.

1. INTRODUCTION

In recent years extensive research has been carried out in the terahertz portion of the electromagnetic spectrum, which is loosely defined as the frequencies from 100 GHz to 30 THz (wavelengths from 3 mm to 10 μm). Traditionally Terahertz science and technology has been applied in space spectroscopy, examining far-infrared radiation, molecular spectroscopy and in the diagnostics of plasma. Today Terahertz science and technology is applied to many more sectors, given the recent advancements and innovations in photonics and nanotechnology[1]. The unique properties of this frequency domain has emerged terahertz technology as a state-of-the-art research field, thus gaining popular interest. However, waveguiding in this intermediate spectral region is a major challenge and strong dielectric and conductive losses in the terahertz frequency range have been a major problem for waveguiding. The conventional guiding structures exemplified by microstrips, coplanar striplines and coplanar waveguides are highly lossy and dispersive, primarily due to lack of materials and devices that respond to terahertz frequencies[2].

The introduction of graphene as a single layer two dimensional atomic crystal of carbon, arranged in a hexagonal honeycomb structure has attracted tremendous interest due to its unique properties[3]. Graphene has been shown to provide supreme material parameters in terms of its chemical, electrical, magnetic and thermal properties[4]. The characteristic material properties of graphene arising from its particular band structure have attracted great attention for terahertz applications. Based on the honeycomb lattice of graphene, the vectors $\mathbf{k} = \left(k_x, k_y\right)$ in the first Brillouin zone (BZ) zone reveal a symmetrical conical shape (Dirac point) located at K and *K'* point[5]. The electronic dispersion in the hexagonal lattice of graphene for finite values of the nearest neighbor hoping energy t is shown in Fig 1. In Fig. 1, the three-dimensional band structure reveals a hexagon with the corners formed at the K points. The excerpt in the figure depicts the low energy dispersion at one of the K points, which shows the electron-hole symmetric Dirac cone structure. The low conical energy dispersion around these K points determines the electronic properties of graphene[6].

Surface plasmons are electromagnetic fields that are formed due to the coupling of free electrons in the interface between a dielectric medium and a conductor. These electron charges can perform coherent fluctuations called surface plasmon oscillations, which is a combination of propagating electromagnetic field and charge density oscillations[7]. The interaction of the free electrons with the electromagnetic field causes surface plasmon polaritons (SPP) that propagate along the interface of the materials and decay evanescently on both sides of the material[8]. In the far-infrared and terahertz ranges graphene can support surface plasmons. Given the fact that the charge density of graphene can be tuned by either electrostatic or chemical doping, graphene can be tuned to support SPP[9].

* c.themistos@cytanet.com.cy; phone +35722394394; fax +35722438567.

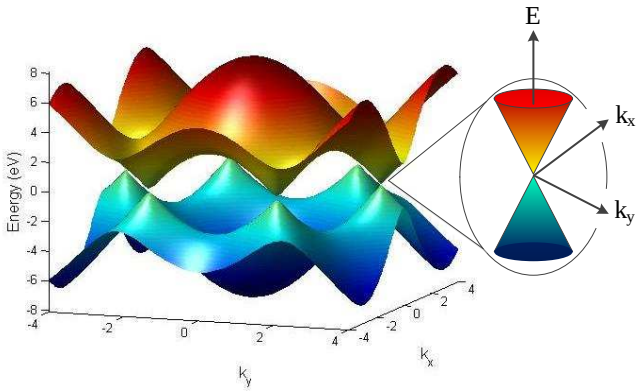

Figure 1. Electronic dispersion in the hexagonal lattice and close up of the energy band close to one of the Dirac points.

2. NUMERICAL ANALYSIS

The Finite Element Method (FEM)[10] has been established as one of the most powerful numerical techniques, because of its accuracy, flexibility and versatility in the numerical analysis of optical waveguides, particularly in structures with arbitrary shapes, index profiles, nonlinearities and anisotropies. In the present work the full vectorial H-field finite element formulation with the aid of perturbation technique[11] has been applied for the modal analysis of the plasmonic waveguide structure, to determine the propagation characteristics of the fundamental and the first higher order mode and to estimate the attenuation characteristics.

The Finite Difference Time Domain method (FDTD) has been regarded as versatile, useful and widely used electromagnetic tool. The performance of the FDTD is embellished with the development of new algorithms to cope with a wide variety of EM problems as well as ABCs[12]. The Auxiliary Differential Equation (ADE) method is applied to study the dispersion characteristics of plasmonic waveguides. The ADE formulation is used in the FDTD algorithm so that the Drude dispersive model can be incorporated in the FDTD field updating equations. The surface conductivity of graphene can be expressed using the Kubo formulation[13]. In this work, the terahertz frequency range considered $\omega \gg 2\mu_c/\hbar$, thus the intraband term becomes negligible, while the dominant interband term takes the form of a Drude-like expression[13]:

$$\sigma(\omega) = \frac{\mathrm{i}\, D_{Gr}}{\pi(\omega + \mathrm{i}\,\Gamma)} \tag{1}$$

where the Drude weight has the form of $D_{Gr} = 2E_F \sigma_{uni}/\hbar$ where E_F is the Fermi energy, $\sigma_{uni} = \pi e^2/2h$ is the universal conductivity of graphene and Γ^{-1} is the damping rate[14].

3. RESULTS

A graphene coated microstrip on Silica substrate has initially been considered in the present analysis, as presented in Fig.2. The complex refractive index, n_g, of the 0.334 nm thick grapheme layer was considered to be, n_g = 30 +j 26 given by Hong et al[15], and the refractive index for Silica substrate n_s to be 1.96 at an operating frequency of 1 THz. The complex refractive index used for the gold (Au) microstrip and the ground plate at the above frequency was considered to be 308 + j532 given by Ordal et al[16]. The 3D FDTD method has been used to model to simulate the 0.5 mm in length microstrip with graphene coating, with $\Delta x = 1\,\mu m$, $\Delta y = 10\,\mu m$, and $\Delta z = 0.25\,\mu m$. The FDTD computational domain was terminated with 10 CPML cells, and the time-step was set to $\Delta t = 72.79$ fs, with a Courant factor of S = 0.9. The relative permittivity for Au was set to ε_r = 9.07, the Drude plasma frequency $\omega_{pD} = 1.2 \times 10^6$ rad/s, the Drude

damping coefficient $\Gamma_D = 1.2\times10^{14}$ rad/s, and the electric conductivity $\sigma = 7.34\times10^{6}$ S/m [17]. The FDTD graphene layer parameters for conductivity were set to $\Gamma_g = 2\times10^{12}$ rad/s, T = 300 K, and $E_f = 0.065$ eV.

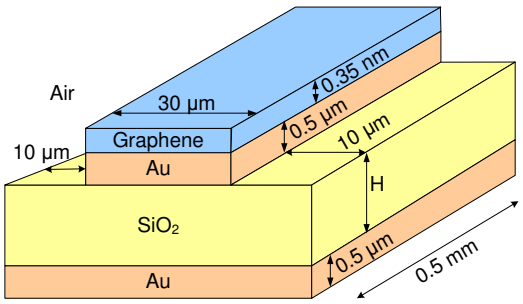

Figure 2. Graphene coated microstrip structure.

Initially, the propagation characteristics of the fundamental quasi-TM like, H_x^0 mode and the first order Surface Plasmon (SP) H_x^{SP} mode, with the variation of the Silica substrate have been studied and presented in Fig.3, where the modal field distributions of the above modes are shown as insets. As can be seen in Fig.3, the effective index decreases with the decreases of the substrate height, H, for both the above modes, with the SP mode exhibiting much higher effective index, above the silica refractive index.

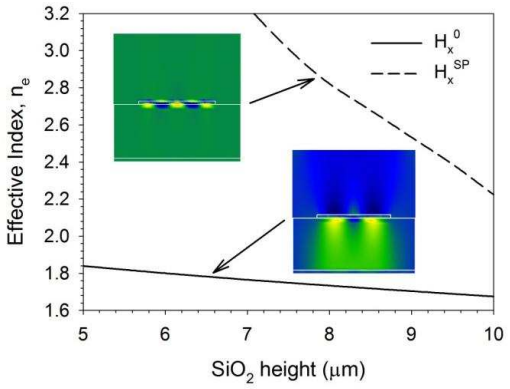

Figure 3. Effective index with the variation of the substrate height, H, for the guided and the first Surface plasmon mode (where the H_x modal fields are shown as insets).

As can be seen from the modal field distribution (shown as insets in Fig.3) the propagation of the H_x field of the fundamental mode is mainly guided within the substrate, while for the SP mode along the gold/Silica interface, therefore the SP modes exhibits high attenuation losses, not presented here.

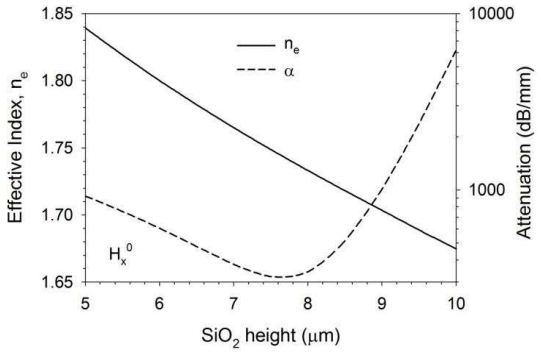

Figure 4. Effective index and attenuation with the variation of the substrate height, H.

Furthermore, the complex propagation characteristics of the guided H_x^0 mode with the variation of the silica substrate height, H, have been examined. From the above curves, shown in Fig.4, it can be seen that both the effective index and the attenuation decrease initially with the increase of the substrate height, H. However, at a substrate height of about 7.6 μm the attenuation exhibits a minimum value of about 320 dB/mm and as the substrate height increases further, it increases rapidly reaching a value of about 1200 dB/mm, at a substrate height of 10 μm.

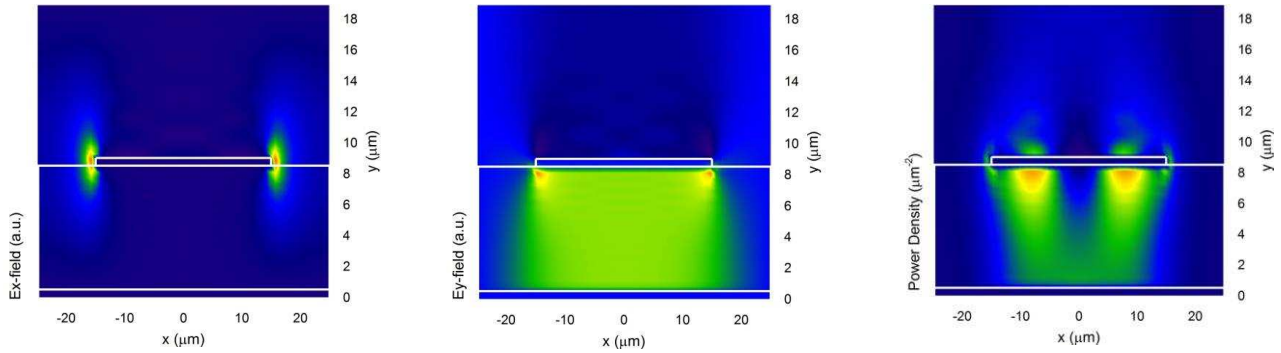

Figure 5. (a) E_x, (b) E_y modal field for the fundamental guided mode, H_x^0 and (c) Power Density for the fundamental guided mode, H_x^0.

The lateral components E_x and E_y of the Electric field modal distribution, for the H_x^0 mode have also been obtained for a substrate height, H, of 8 μm and presented in Fig.5(a) and (b), respectively. As can be seen from the above field distributions, for the E_x field the field distribution is concentrated at the sides of the microstrip, while the E_y field is concentrated below the Au/SiO_2 interface and extending in the substrate region. The Power density for the H_x^0 mode for a substrate height of 8 μm has also been calculated and presented in Fig. 5(c), where it can be observed that the Power is mainly concentrated close to the Au/SiO_2 interface, mainly from the contribution of the H_x field, which is the dominant component in the above mode. The FEM results of the modal fields for the fundamental guided mode in Fig. 5 are also in good agreement with the FDTD simulations (not shown here).

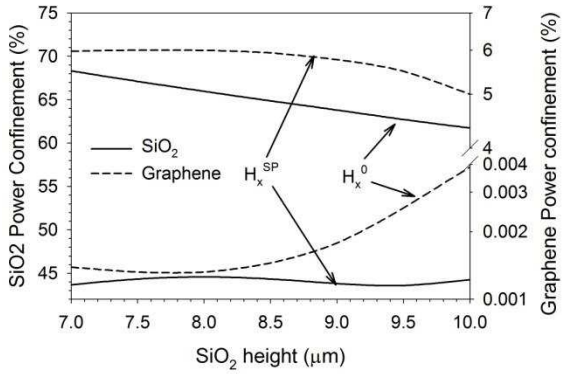

Figure 6. Power Confinement with the variation of the substrate height, H, in the Silica and Graphene Region for the guided and the first Surface plasmon mode.

Next, the variation of the Power confinement in the silica and grapheme region, for the fundamental H_x^0 mode and the H_x^{SP}, first order SP mode with the substrate height, H, has also been calculated and presented in Figure 6. As can be seen from the above characteristics, the power confinement for the H_x^0 is higher in the silica region than in the grapheme layer. As the silica height increases, the power confinement in the silica region decreases, while the power in the grapheme region increases. On the other hand, for the H_x^{SP} mode the power confinement is much lower in the silica substrate region and remains almost constant with the increase of the substrate height. However, the power in the grapheme layer, which is much higher for the H_x^{SP}, decreases slightly with the increase of the substrate height.

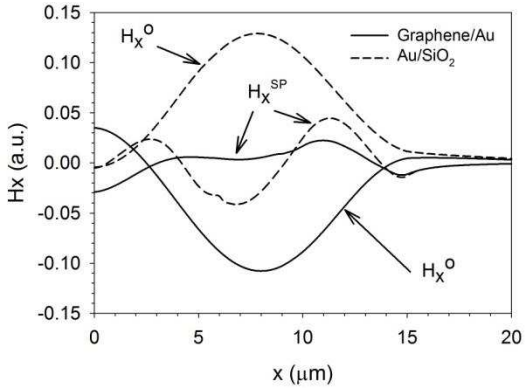

Figure 7. Variation of the H_x along the x-axis for for the guided and the first Surface plasmon mode.

The H_x field profile along the x-axis, for the H_x^0 and the H_x^{SP} mode has also been recorded and presented in figure 7, where the variation of the H_x field along the Graphene/Au and the Au/SiO_2 interfaces is presented.

During the FDTD simulations the electric field was monitored at different locations along the direction of propagation of the Gaussian pulse. At the end of the simulation the Discrete Fourier Transforms (DFT) of the electric fields were calculated. The ratio of the DFT electric fields at different locations is used to calculate the complex propagation constant. At 1 THz, both the FEM and FDTD simulations have shown that the complex propagation constant is 35 rad/mm. In Fig. 8 the propagation constant for various substrate heights is plotted between 0.5 and 1.8 THz. Based on the results presented in Fig. 8 the propagation constant remains the same up to 1 THz for all substrate heights. At higher frequencies the propagation constant deviates for most substrate heights, where as for a substrate height of 9 mm, the trend appears to be linear.

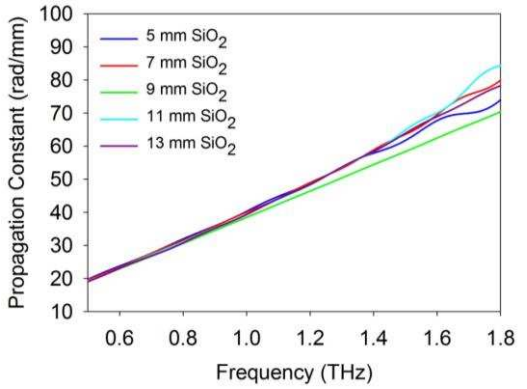

Figure 8. Propagation constant for microstrip structure.

In Fig. 9 the characteristic impedance for a range of frequencies between 0.5 and 1.8 THz is plotted for different substrate heights. During the FDTD simulations, the current on the surface of the graphene layer and the voltage across the microstrip and the ground plate were monitored. The characteristic impedance of the microstrip can then be calculated using the DFT frequency domain values of the voltage and current values. Based on the results in Fig. 9, as the substrate height increases from 5 to 13 mm, the real value of the characteristic impedance is also increased, whereas for the imaginary value of the characteristic impedance, as the substrate height increases the imaginary value decreases. Also, it appears that at higher frequencies the values for all substrate heights, for both the real and the imaginary part of the characteristic impedance, seem to converge.

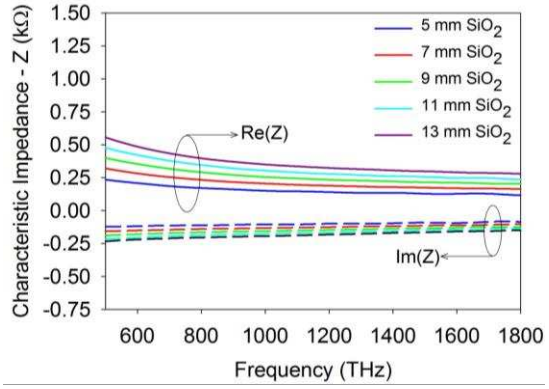

Figure 9. Characteristic Impedance for microstrip structure.

4. CONCLUSION

A graphene coated microstrip is presented capable of supporting SPPs for Terahertz propagation. The plasmonic behavior of the waveguide is analyzed using the full vectorial FEM and the FDTD method. The modal properties of the microstrip structure have been presented with emphasis on the SPM. Moreover, the FDTD method has been used as a numerical analysis tool for evaluating the electric field distribution and determining the dispersion characteristics of the microstrip structure. Graphene has emerged as the ultimate material for the terahertz frequency range due to its unique properties. It has been demonstrated that a graphene layer can support SPP, and graphene plasmonics may enable in the future a wide variety terahertz devices for communications to spectroscopy applications.

REFERENCES

[1] M. Tonouchi, "Cutting-edge terahertz technology," Nat Photon, vol. 1, pp. 97-105, 2007.

[2] P. H. Siegel, "Terahertz technology," Microwave Theory and Techniques, IEEE Transactions on, vol. 50, pp. 910-928, 2002.

[3] K. S. Novoselov, A. K. Geim, S. V. Morozov, D. Jiang, Y. Zhang, S. V. Dubonos, I. V. Grigorieva, and A. A. Firsov, "Electric Field Effect in Atomically Thin Carbon Films," Science, vol. 306, pp. 666-669, October 22, 2004 2004.

[4] K. S. Novoselov, V. I. Falko, L. Colombo, P. R. Gellert, M. G. Schwab, and K. Kim, "A roadmap for graphene," Nature, vol. 490, pp. 192-200, 2012.

[5] A. H. Castro Neto, Guinea, F., Peres, N. M. R., Novoselov, K. S. and Geim, A. K., "The electronic properties of graphene," Rev. Mod. Phys., vol. 81, pp. 109-162, 2009.

[6] E. Y. Andrei, G. Li, and X. Du, "Electronic properties of graphene: a perspective from scanning tunneling microscopy and magnetotransport," Reports on Progress in Physics, vol. 75, p. 056501, 2012.

[7] H. Raether, Surface plasmons on smooth and rough surfaces and on gratings. Berlin ; New York: Springer-Verlag, 1988.

[8] D. Sarid and W. A. Challener, Modern introduction to surface plasmons : theory, Mathematica modeling, and applications. Cambridge ; New York: Cambridge University Press, 2010.

[9] A. N. Grigorenko, M. Polini, and K. S. Novoselov, "Graphene plasmonics," Nat Photon, vol. 6, pp. 749-758, 2012.

[10] B. M. A. Rahman and J. Davies, "Finite-element solution of integrated optical waveguides," Lightwave Technology, Journal of, vol. 2, pp. 682-688, 1984.

[11] C. Themistos, B. M. A. Rahman, and K. T. V. Grattan, "Finite element analysis for lossy optical waveguides by using perturbation techniques," Photonics Technology Letters, IEEE, vol. 6, pp. 537-539, 1994.

[12] A. Taflove and S. C. Hagness, Computational Electrodynamics: The Finite-Difference Time-Domain Method, 3 ed.: Artech House Publishers, 2005.

[13] G. W. Hanson, "Dyadic Green's functions and guided surface waves for a surface conductivity model of graphene," Journal of Applied Physics, vol. 103, pp. 064302-064302-8, 2008.
[14] P. Avouris and M. Freitag, "Graphene Photonics, Plasmonics, and Optoelectronics," Selected Topics in Quantum Electronics, IEEE Journal of, vol. 20, pp. 72-83, 2014.
[15] J. T. Hong, K. M. Lee, B. H. Son, S. J. Park, D. J. Park, J.-Y. Park, S. Lee, and Y. H. Ahn, "Terahertz conductivity of reduced graphene oxide films," Optics Express, vol. 21, pp. 7633-7640, 2013.
[16] M. A. Ordal, L. L. Long, R. J. Bell, S. E. Bell, R. R. Bell, R. W. Alexander, and C. A. Ward, "Optical properties of the metals Al, Co, Cu, Au, Fe, Pb, Ni, Pd, Pt, Ag, Ti, and W in the infrared and far infrared," Applied Optics, vol. 22, pp. 1099-1119, 1983.
[17] A. Vial, A.-S. Grimault, D. Macias, D. Barchiesi, and M. L. de la Chapelle, "Improved analytical fit of gold dispersion: Application to the modeling of extinction spectra with a finite-difference time-domain method," Physical Review B, vol. 71, p. 085416, 2005.